Spontaneous formation of dye-functionalized gold nanoparticles using reverse micellar systems

Masaki Takahashi,[a,] Shuhei Ohno,[a] Norifumi Fujita[†,b] Tetsuya Sengoku[a] and Hidemi Yoda[a,*]*

[a]Department of Materials Science, Faculty of Engineering, Shizuoka University, 3-5-1 Johoku, Naka-ku, Hamamatsu, Shizuoka 432-8561, Japan

[b]Department of Chemistry and Biochemistry, Graduate School of Engineering, Kyushu University, 744 Moto-oka, Nishi-ku, Fukuoka 819-0395, Japan

[†]*Present address*: Department of Chemistry and Biotechnology School of Engineering, The University of Tokyo, 7-3-1 Hongo, Bunkyo-ku, Tokyo 113-8656, Japan.

Tel: +81-53-478-1621; FAX: +81-53-478-1621; e-mail address: tmtakah@ipc.shizuoka.ac.jp

Tel: +81-53-478-1150; FAX: +81-53-478-1150; e-mail address: tchyoda@ipc.shizuoka.ac.jp

Abstract

Detailed exploratory and mechanistic investigations on spontaneous formation of dye-functionalized gold nanoparticles (GNPs) using dye-based reverse micellar systems are described in this publication. The accumulated results from spectroscopic and microscopic investigations demonstrated that water molecules confined within nanoscopic enclosure of the self-assembled reverse micelles played critical role in the redox processes of aurate ions to produce GNPs, which are assumed to have approximately constant size distributions. The resulting dye-functionalized GNPs were found to offer their absorption and fluorescence emission tunability by changing the medium polarity as well as to exhibit excellent film-forming properties to give optically homogeneous polystyrene thin films. These key findings in addition to broad applicability of the self-assembling process with a variety of dye analogues have led to a conclusion that the protocol presented here serves as a versatile synthetic method to provide a potential convenience for future development of new organic-inorganic hybrid nanomaterials.

Abbreviations

GNP: gold nanoparticle

NTCA: naphthalene-1,4,5,8-tetracarboxylic dianhydride

PTCA: perylene-3,4,9,10-tetracarboxylic dianhydride

NMP: N-methylpyrrolidone

THF: tetrahydrofuran

SPR: surface plasmon resonance

W_0: molar ratio of water to dye molecules

t_s: sonication time for complexation of dye with $HAuCl_4$

t_i: incubation time for complexation of dye with $HAuCl_4$

r: stoichiometric ratio of $HAuCl_4$/dye

1. Introduction

Hybrid nanomaterials, composed of both organic and inorganic components, have attracted a great deal of interest in the past few years as advanced materials with desirable optical, electrical and magnetic properties [1], which have been employed for several emerging applications such as imaging agents [2], semiconductors [3-5] and photoelectric devices [6-8]. Engineering surfaces of inorganic nanomaterials with functional dyes provides the ability to independently tune the energy levels of each component, and thus will pave the way for the development of new photonic devices with finely-tuned optoelectronic properties [9,10]. On the basis of the idea that the rapidly emerging field of the plasmonics can be applied to construction of not only superior photonic devices based on surface electromagnetic field enhancement [11, 12], but also efficient solar energy conversion systems [13], considerable effort has been devoted to develop efficient synthetic routes for the generation of organic-inorganic hybrid nanomaterials [14-16]. In a previous publication, we have discovered spontaneous formation of organic-inorganic hybrid gold nanoparticles (GNPs) through treatment of trichromophoric light-harvesting dye **1**, which has been designed to funnel absorbed photons from anthracene units to perylene core [17], with aqueous hydrogen tetrachloroaurate in toluene (Scheme 1) [18]. Of particular interest in this context is demonstration that the gold cations of the dye-aurate salts were spontaneously reduced in the absence of any reducing agents to give the GNPs, accompanied by self-assembly of the protonated dyes into spherically shaped reverse micelles, where the gold nanoparticles would be encapsulated within the reverse micellar shells. Driven by these intriguing findings, we decided to pursue our research on this poorly understood phenomenon to gain insight into the mechanism and the scope of these chemical processes in more details as well as to show broad applicability of this protocol as a potential method for the synthesis of many types

of organic-inorganic hybrid nanomaterials. In the present publication, we describe the complete details of exploratory and mechanistic investigations on the production of the dye-functionalized GNPs by the use of the trichromophoric dye **1** and related analogues **2-5** (Fig. 1).
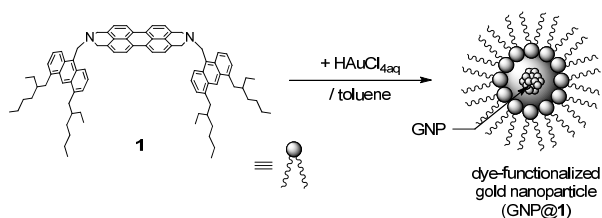
Scheme 1. Schematic representation of the production of the dye-functionalized GNPs from **1**.
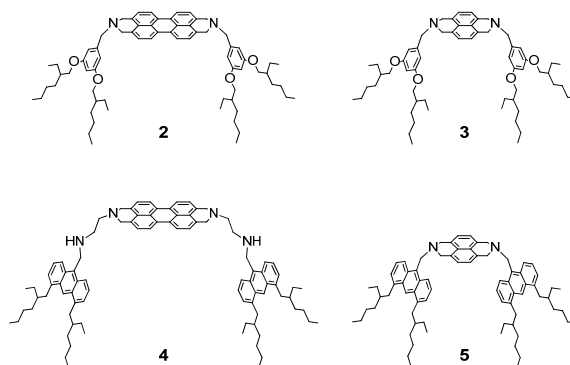
Fig. 1. Structures of dyes **2-5**.

2. Material and methods

2.1. General

All solvents and reagents were of reagent grade quality from Wako Pure Chemicals and Tokyo Chemical Industry (TCI) used without further purification, except for polystyrene beads with average molecular weight of 250,000 from Acros Organics. The ^{1}H and ^{13}C nuclear magnetic resonance (NMR) spectra operating at the frequencies of 300 and 75 MHz, respectively, were recorded on a JEOL JNM-AL300 spectrometer in chloroform-d (CDCl$_3$). Chemical shifts are reported in parts per million (ppm) relative to TMS and the solvent used as internal standards, and the coupling constants are reported in hertz (Hz). Fourier transform infrared (FTIR) spectra were recorded on a JASCO

FT/IR-4100 spectrometer. UV-vis and fluorescence (excitation) spectra were recorded on a JASCO V-530 spectrophotometer and a JASCO FP-6200 spectrofluorometer, respectively. Elemental analyses were performed by JSL Model JM 10 instruments. The atomic force microscope (AFM) analyses were performed on a Veeco NanoScope IIIa microscope for GNP@**3** and a Keyence VN-8010 for all other samples. The trichromophoric dye **1** and the two related analogues **2** and **5** were prepared according to already published reaction protocol and used for experiments [17, 19]. The other materials **3** and **4** were synthesized as described in the following procedures.

2.2. Materials

*2.2.1. Synthetic procedure for **9***

A solution containing 9-(chloromethyl)-4,5-bis(2-ethylhexyl)anthracene **8** (0.100 g, 0.222 mmol) in THF (10 mL) was added to vigorously stirred ethylene diamine (5 mL) at room temperature under nitrogen atmosphere. After 2 hours, the reaction mixture was quenched by addition of water (50 mL), and extracted with hexane (50 mL). The organic layer was washed with brine (30 mL), dried over anhydrous Na_2SO_4. The filtrate was concentrated *in vacuo* to gave the corresponding diamine derivative **9** (0.198 g, 85%) as a yellow oil: IR (NaCl) 3266 cm^{-1} (N-H), 3299 cm^{-1} (N-H), 1617 cm^{-1} (C=C); ^{1}H NMR δ 8.84 (s, 1H, Ar*H*), 8.21 (d, *J* = 9.0 Hz, 2H, Ar*H*), 7.33 (dd, *J* = 9.0, 5.4 Hz, 2H, Ar*H*), 7.27 (d, *J* = 5.4 Hz, 2H, Ar*H*), 4.71 (s, 2H, C*H₂*), 3.27 (d, *J* = 7.4 Hz, 4H, C*H₂*), 3.13 (dd, *J* = 7.2, 14.1 Hz, 4H, C*H₂*), 2.95 (t, *J* = 5.4 Hz, 2H, C*H₂*), 2.85 (t, *J* = 5.4 Hz, 2H, C*H₂*), 2.0−1.9 (m, 2H, C*H*), 1.5−1.2 (m, 19H, C*H₂*, N*H*, N*H₂*), 0.9−0.8 (m, 12H, *Me*); ^{13}C NMR δ 138.7 (*C*) 132.6 (*C*), 130.3 (*C*), 125.9 (*C*), 125.9 (*C*), 125.6 (*CH*), 122.4 (*CH*), 119.6 (*CH*), 53.1 (*CH₂*), 46.3 (*CH₂*), 41.8 (*CH₂*), 39.7 (*CH*), 38.5 (*CH₂*), 32.6 (*CH₂*), 28.9 (*CH₂*), 25.6 (*CH₂*), 23.1 (*CH₂*), 14.0 (*CH₃*), 10.5 (*CH₃*). Anal. Calcd for $C_{33}H_{50}N_2$: C, 83.48; H, 10.62; N, 5.90. Found: C, 83.72; H, 10.31; N, 6.02.

*2.2.2. Synthetic procedure for **7***

A solution containing 3,5-bis(2-ethylhexyloxy)benzylamine **6** (1.05 g, 2.89 mmol) and NTCA (0.260 g, 0.969 mmol) in NMP (30 mL) was heated at 110 °C with stirring under argon atmosphere. After 3 hours, the reaction mixture was cooled to room temperature, quenched by addition of water (50 mL), and then extracted with hexane (50 mL). The organic layer was washed with water (100 mL) and brine (20 mL), dried over anhydrous Na_2SO_4, filtered, and concentrated *in vacuo*. The residue was purified by silica-gel column chromatography (hexane/ethyl acetate = 10/1) to gave **7** (0.498 g, 0.519 mmol, 54%) as a yellow solid: IR (NaCl) 3018 cm^{-1} (C-H), 2961 cm^{-1} (C-H), 2928 cm^{-1} (C-H), 1706 cm^{-1} (C=O), 1670 cm^{-1} (C=C); ^{1}H NMR δ 8.77 (s, 4H, Ar*H*), 6.64 (d, *J* = 2.2 Hz, 4H, Ar*H*), 6.35 (t, *J* = 2.2 Hz, 2H, Ar*H*), 5.31 (s, 4H, C*H*$_2$), 3.79 (dd, *J* = 5.7, 15.3 Hz, 8H, C*H*$_2$), 1.7-1.6 (m, 4H, C*H*), 1.5-1.3 (m, 28H, C*H*$_2$), 0.9-0.8 (m, 24H, *Me*); ^{13}C NMR δ 162.9, 160.7, 138.5, 131.2, 126.8, 107.3, 100.5, 70.4, 44.0, 39.3, 30.4, 29.0, 23.7, 22.9, 14.0, 11.0. Anal. Calcd for $C_{60}H_{82}N_2O_8$: C, 75.12; H, 8.62; N, 2.92. Found: C,75.27; H, 8.37; N, 3.02.

2.2.3. Synthetic procedure for **10**

Following the procedure for the synthesis of **7**, employing **9** (0.600 g, 1.27 mmol) with PTCA (0.166 g, 0.424 mmol), afforded **10** (0.333 g, 0.267 mmol, 50%) as a dark brown solid after column chromatography (chloroform/methanol = 20/1): IR (NaCl) 3020 cm^{-1} (C-H), 2960 cm^{-1} (C-H), 2926 cm^{-1} (C-H), 1694 cm^{-1} (C=O), 1654 cm^{-1} (C=C); ^{1}H NMR δ 8.71 (s, 1H, Ar*H*), 8.53 (d, *J* = 8.1 Hz, 2H, Ar*H*), 8.37 (d, *J* = 9.0 Hz, 2H, Ar*H*), 8.25 (d, *J* = 9.0 Hz, 2H, Ar*H*), 7.37 (dd, *J* = 6.6, 8.1 Hz, 2H, Ar*H*), 7.19 (d, *J* = 6.6 Hz, 2H, Ar*H*), 4.83 (s, 2H, C*H*$_2$), 3.34 (t, *J* = 6.3 Hz, 4H, C*H*$_2$), 3.34 (t, *J* = 7.4 Hz, 4H, C*H*$_2$), 3.04 (dd, *J* = 7.5, 15.0 Hz, 8H, C*H*$_2$), 2.0−1.9 (m, 4H, C*H*), 1.5−1.2 (m, 34H, C*H*$_2$, N*H*), 0.9-0.8 (m, 24H, *Me*). Anal. Calcd for $C_{90}H_{104}N_4O_4$: C,82.78; H, 8.03; N, 4.29. Found: C, 82.53; H, 7.74; N, 4.62.

2.2.4. Synthetic procedure for **3**

To a solution of aluminum chloride (0.150 g, 1.12 mmol) in anhydrous THF (5 mL) was added lithium aluminum hydride (0.043 g, 1.1 mmol) in small portions at 0 ˚C for 30 min. After removal of the ice-bath and stirring for additional 30 min, a solution of **7** (0.030 g, 0.028 mmol) in anhydrous THF (5 mL) was added and the reaction mixture was stirred at room temperature. After 2 hours, the resulting reaction mixture was quenched with water (3 mL) and 3% aqueous HCl (3 mL) at 0 ˚C. To the residue was added 10 wt % NaOH (10 mL) and the resulting oil was dissolved in hexane (50 mL), washed with water (50 mL) and brine (50 mL). The organic layer was dried over Na_2SO_4, filtered, and concentrated *in vacuo* to give **3** (25 mg, 2.7 mmol, 95%) as a colorless oil: IR (NaCl) 3020 cm^{-1} (C-H), 2962 cm^{-1} (C-H), 2929 cm^{-1}; ^{1}H NMR δ 7.09 (s, 4H, Ar*H*), 6.54 (d, *J* = 2.2 Hz, 4H, Ar*H*), 6.39 (t, *J* = 2.2 Hz, 2H, Ar*H*), 3.95 (s, 8H, C*H₂*), 3.79 (dd, *J* = 5.7, 15.3 Hz, C*H₂*), 3,70 (s, 4H, C*H₂*), 1.7-1.64 (m, 4H, C*H*), 1.5-1.3 (m, 28H, C*H₂*), 0.9-0.8 (m, 28H, *Me*); ^{13}C NMR δ 160.7, 14.5, 131.7, 127.8, 107.3, 100.3, 70.5, 62.1, 56.4, 39.4, 30.5, 29.0, 23.8, 22.9, 14.0, 11.0. Anal. Calcd for $C_{60}H_{90}N_2O_4$: C, 79.77; H, 10.04; N, 3.10. Found: C,79.88; H, 9.65; N, 3.34.

2.2.5. Synthetic procedure for 4

Following the procedure for the synthesis of **3** employing **10** (0.030 g, 0.028 mmol) afforded **4** (0.025 g, 0.024 mmol, 87%) as a yellow solid after column chromatography (chloroform/methanol = 50/1): IR (NaCl) 3020 cm^{-1} (C-H), 2959 cm^{-1} (C-H), 2929 cm^{-1} (C-H); HRMS (ESI) *m/z* calcd for $C_{90}H_{113}N_4$: 1249.8965, found 1249.8882; ^{1}H NMR δ 8.82 (s, 2H, Ar*H*), 8.21 (d, *J* = 9.0 Hz, 4H, Ar*H*), 8.02 (d, *J* = 7.5 Hz, 4H, Ar*H*), 7.29 (dd, *J* = 6.7 and 9.0 Hz, 4H, Ar*H*), 7.21 (d, *J* = 6.7 Hz, 4H, Ar*H*), 7.09 (d, *J* = 7.5 Hz, 4H, Ar*H*), 4.83 (s, 4H, C*H₂*), 4.12 (s, 8H, C*H₂*), 3.2-3.1 (m, 12H, *CH₂*), 2.86 (t, *J* = 5.1 Hz, 5H, C*H₂*) 2.0-1.9 (m, 4H, C*H*), 1.5−1.2 (m, 32H, C*H₂*), 1.0−0.8 (m, 24H, *Me*); ^{13}C NMR δ 138.6, 132.7, 130.5, 130.2, 130.0, 129.3, 128.2, 126.0, 125.7, 123.1, 122.4, 120.0, 119.3, 67.9, 56.2, 46.9, 39.7, 38.5, 38.4, 32.6, 28.6, 25.6, 25.5, 23.1, 14.0, 10.5.

2.3. Typical experimental procedure for the complexation of dyes with HAuCl$_4$

In a typical experimental procedure, a toluene solution containing 1.0 mM concentration of the dye (c = 1.0 mM (0.5 mM for the case of **4**)) was treated with aqueous HAuCl$_4$ (stoichiometric ratio of HAuCl$_4$/dye: r = 4.0 equiv (6.0 equiv for the case of **4**)) by use of a micropipette, where the molar ratio of water to the dye equals to 50 (W_0 = 50). A clear solution prepared by sonication of the mixture for 3 min (t_s = 3 min) was incubated over a period of 6 hours (t_i = 6 h (28 h for the case of **4**)) at room temperature. This is taken as standard conditions for each complexation experiment.

2.4. Typical experimental procedure for AFM analyses

In a typical experimental procedure, the reaction mixture diluted with dry toluene (c = 0.1 mM) was drop-cast on to the HOPG. Airdried sample of the reaction mixture was examined by carrying out measurements in tapping mode.

2.5. Typical experimental procedure for GNP-doped polystyrene films

In a typical experimental procedure, to a toluene solution containing 1.0 mM concentration of the dye-functionalized GNPs was added polystyrene beads (average molecular weight: 250,000) at a concentration of 0.1 g/mL. A solution obtained by stirring the mixture was then drop-cast on a piece of glass plate, which was airdried at room temperature to give reproducibly homogeneous thin films.

3. Results and discussion

3.1. Preparation of new dyes

As a starting point for this study, we set out to prepare the new dye analogues **3** and **4** which share the common nonconjugated backbone structures based on rigid aromatic units and 2-ethylhexyl side chains. The synthesis of these compounds was performed according to the established literature procedure [19]. Two types of arylmethyl amines **6** and **9** envisioned as prerequisite synthetic intermediates were readily available from our preliminary study and by substitution reaction of 9-

(chloromethyl)-4,5-bis(2-ethylhexyl)anthracene **8** with ethylene diamine, respectively (Scheme 2). Condensation of these primary amines **6** and **9** with NTCA and PTCA gave the corresponding bisimides **7** and **10**, whose imide functionalities were completely reduced to tertiary amino groups upon treatment with aluminum hydride, giving rise to the desired dyes **3** and **4** in analytically pure forms, respectively.
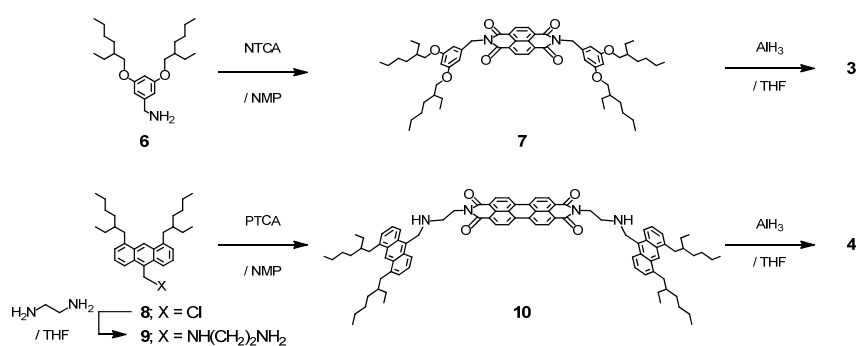
Scheme 2. Preparation of **3** and **4**.

3.2. Spectral behavior of dye-functionalized GNPs

It has been demonstrated that the prototypical dye **1** afforded reproducibly the corresponding dye-functionalized GNPs (designated as GNP@**1**) upon complexation with $HAuCl_4$ in toluene under the standard conditions [18]. As has previously been observed by the UV-vis spectroscopy, the resulting solutions exhibited discernible broadening and bathochromic shift of the absorption peaks due to the aggregated nature of the dyes along with the appearance of the SPR band at 518 nm, which are characteristics of extremely small-sized GNPs (Fig. 2A). Furthermore, steady-state fluorescence measurements of the solutions upon excitation at 368 nm, where direct excitation of the anthracene chromophores was more likely, showed strong fluorescence quenching of both the excited anthracene and the perylene groups (Fig. 2B). This quenching behavior could be explained in terms of the radiationless deactivation governed primarily by efficient energy transfer from the excited anthracene to the perylene groups [17] and electron transfer from the GNPs to the excited perylene

groups [18, 20], demonstrating that GNPs should be formed within the reverse micellar shells of the dyes.
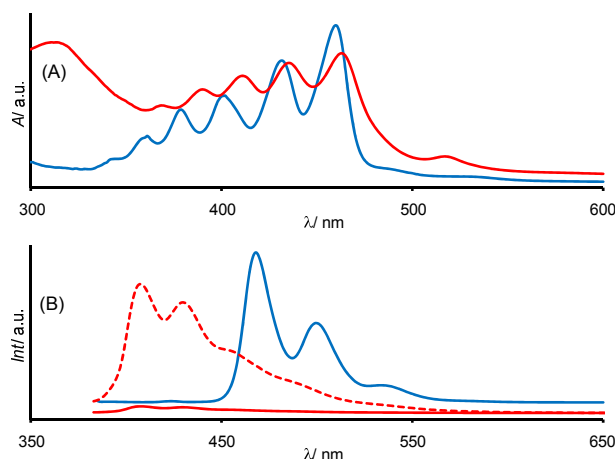
Fig. 2. (A) Absorption (c = 10.0 μM) and (B) fluorescence (λ_{ex} = 368 nm, c 0.1 μM) spectra of **1** (blue) and dye-functionalized GNPs (red) in toluene. Red dotted line represents the enlarged fluorescence spectrum of the dye-functionalized GNPs in toluene.

3.3. Effects of concentration and stoichiometric ratio on the GNP formations

In an initial attempt to resolve experimentally fundamental mechanistic aspect of the spontaneous formation of the GNPs, we tested several samples to check reproducibility of the results with varying the initial concentration of **1** (c) and keeping all other factors constant (t_s = 3 min, t_i = 6 h, r = 4.0 equiv, W_0 = 50). When the change in relative absorbance at 518 nm was monitored as a function of the concentration, we found that there existed a threshold level between 0.3 and 0.4 mM, where the distinguishable SPR band appeared (Fig. 3). Based on this consideration, the only assumption here is that the self-assembly of the diprotonated **1** into the reverse micelles should be an essential prerequisite for the spontaneous formation of the GNPs. This was confirmed by the observation that no SPR band could be detected when we added $HAuCl_4$ to the solution of **1** in stoichiometric ratios less than the theoretically ideal value required for the diprotonation ($r < 2.0$, c = 1.0 mM, t_s = 3 min, t_i = 6 h, W_0 = 50, details in the Supplementary material, see Fig. S1). At the r values higher than 2.7, there appeared distinct maxima of the absorption bands whose resonance wavelength and relative

10

absorbance remained essentially unchanged throughout this spectrophotometric titrations ($r \leq 100$). These results indicate the self-assembly of the reverse micelles plays an important role in the spontaneous formations of the GNPs shown to have an approximately constant size distribution independent of the amount of HAuCl$_4$ added. The observed particle size control may be understood in terms of occupation of the hydrophilic pocket of the reverse micelles by aurate ions. In this context, we have previously shown that the reverse micelles obtained through treatment of **1** with sulfuric acid have a uniform aggregate size unaffected by water content due to steric constraints and molecular rigidity of the polyaromatic system [17]. From this, it can be deduced that initially formed reverse micelles could encapsulate only a limited amount of aurate ions in the hydrophilic pocket to undergo the reaction, expelling extra HAuCl$_4$ through the volume effect.
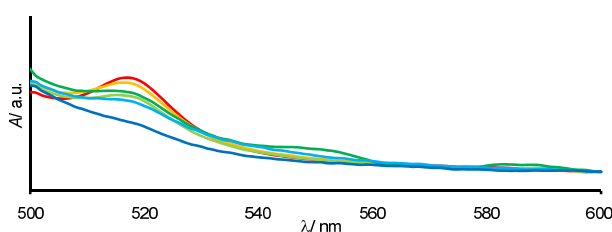
Fig. 3. Absorption spectra of **1**-HAuCl$_4$ complexes in toluene at the *c* values of 0.1 (blue), 0.2 (light blue), 0.3 (green), 0.4 (light green), 0.5 (orange) and 1.0 mM (red) after incubation for 6 h.

3.4. Effects of water content on the GNP formations

Of mechanistic relevance in the particle size control is a study of the influence of the water content on the shape of the absorption spectra as a function of W_0 values. As expected from the foregoing discussion, the spectra showed no significant change in the position of the SPR band when the sample preparations were carried out with varying the W_0 values from 50 to 100 at a fixed set of standard conditions ($c = 1.0$ mM, $r = 4.0$, $t_s = 3$ min, $t_i = 6$ h, details in the Supplementary material, see Fig. S2). These results demonstrated that the confined aqueous environment within the reverse micelles should expel extra water to maintain the constant aggregate form, resulting in the size

control to yield the uniformly sized GNPs. Another remarkable result from this experiment was that attempts to generate GNPs at lower W_0 values of 10, 20 and 30 failed as evidenced by the lack of the SPR band. It may be suggested that a certain amount of water confined within the reverse micellar enclosure would be required to promote the redox processes involved in the GNP formation.

3.5. Reproducibility of dye molecules

The above observations prompted us to identify oxidized species supplying electrons to aurate ions throughout the reduction processes. Assuming that the molecular shells of the reverse micelles would be oxidized, we attempted to recover **1** from the dye-functionalized GNPs to confirm its stability toward the oxidative degradation. In this experiment, we carried out dark incubation of GNP@**1** for 10 days at room temperature after the sample preparation under the standard conditions ($c = 1.0$ mM, $r = 4.0$, $t_s = 3$ min, $t_i = 6$ h, $W_0 = 50$), followed by treatment with 10% aqueous NaOH and complete removal of released GNPs by filtration through Celite. Finally, extraction of the filtrate with toluene and concentration of the combined organic extracts gave quantitative recovery of **1**, which was subjected to ^{1}H NMR analysis. Comparison of the ^{1}H NMR spectrum with the literature data [17] gave unambiguous proof for the chemical integrity of the regenerated **1** (details in the Supplementary material, see Fig. S3), and therefore it is unlikely that degradation of the molecular shells is involved in the redox processes. Based on this consideration, another mechanistic possibility was that the reaction could be promoted by special reactivity of the encaged water molecules.

3.6. Effects of additives on the GNP formations

In order to address the question concerning this reactivity, we explored an approach using aqueous ethylene glycol and glycerol as alternative agents for solubilization of aurate ions. In practice, these polyols would be easily oxidized and present in the hydrophilic pocket of the reverse micelles due to the insolubility in most nonaqueous media, allowing exploration of their associated effects on the

reaction rate. Thus, the experiments were carried out with a mixture of the polyols and aqueous

HAuCl$_4$ at a molar ratio of the polyols to water as 1:1 so that we could compare the time courses of

the reaction with a control sample prepared by the standard procedure (c = 1.0 mM, r = 4.0, t_s = 3

min, W_0 = 50). At an early stage of the reaction (t_i = 3 h), the solutions prepared with ethylene glycol

and glycerol showed remarkable increases in relative absorbances at 518 nm, which were about 3.3-

and 2.9-fold higher than that of the control sample, respectively (details in the Supplementary

material, see Fig. S4). The observed enhancement of the respective absorbances can only be

attributed to favorable redox properties of the polyols confined within the reverse micelles, which are

suggested to play a significant role in the progression of the GNP growth [21, 22]. These results

strongly indicate the possibility that hydroxyl-bearing substrates such as water and polyols are

potentially susceptible to oxidative processes and promote the spontaneous formation of the GNPs

when they are confined within the nanoscopic enclosure of the reverse micelles. Recently,

tryptophan-based amphiphiles has been demonstrated to produce thermally stable GNPs through in

situ reduction of aurate ions, where a mechanism involving reduction with the tryptophan moiety

would provide the most reasonable explanation for the spontaneous GNP formation [23]. In light of

the similarity of the above behavior to that observed in our system, it may be likewise inferred that

the tertiary amino groups in **1** would mediate the redox processes between aurate ions and the

hydroxyl-bearing species.

3.6. Solvent effects on the spectral behavior

   During the foregoing discussion, our proposed model for the dye-functionalized GNPs has been

developed by assuming that the spontaneously formed GNPs were surrounded by spherical arrays of

the self-assembling dye molecules, where the perylene moieties would be bound to the surface of the

GNPs with the anthracene units being relatively oriented away from the GNPs. In agreement with

this proposal, fluorescence of the perylene chromophores was more strongly quenched in the toluene

medium due to electron transfer from the GNPs in comparison with that of the anthracene chromophores, as seen in Fig. 2B [18]. In this regard, remarkable changes in the absorption and fluorescence emission behavior occurred when more polar solvent systems were used for the spectral measurements (Fig. 4). With mixed solvents of toluene and ethanol in various ratios (5-35% v/v), a progressive blue shift of the absorption maxima was observed at higher solvent polarity as the local molecular environment became more polar, where the spectra hold clear SPR peaks shifting to 510 nm (Fig. 4A). Furthermore, under these solvent conditions, pronounced fluorescence emissions assignable to monomeric perylene species appeared in the wavelength region of 450-550 nm, whose intensities increased significantly with increasing solvent polarity, accompanying appearance of weak anthracene emissions in the wavelength region of 400-450 nm (Fig. 4B). These observations suggest that GNP@**1** changed their bulk specific volumes without diffusion of the self-assembled molecular arrays to attenuate electron transfer quenching, probably due to greater solvent swelling in the mixed solvent systems. Considering that the fluorescence behavior of the perylene chromophores were much more affected by the change of solvent polarity than that of the anthracene chromophores, it appeared that the perylene chromophores would be in close contact with the GNPs to interact much more than the anthracene chromophores in this dye/GNP aggregate system. Thus, in addition to some improvement in our understanding of the structural description of GNP@**1**, the results described above are quite remarkable and demonstrate this hybrid system can provide the ability to tune its absorption and fluorescence emission characteristics simply by changing the medium polarity.
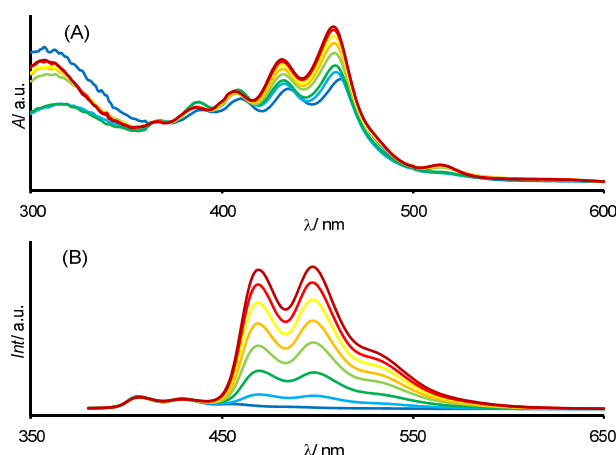
Fig. 4. (A) Absorption (c = 10.0 μM) and (B) fluorescence (λ_{ex} = 368 nm, c = 0.1 μM) spectra of dye-functionalized GNPs diluted with toluene (blue) and a mixture of 5% (light blue), 8% (green), 15% (light green), 20% (orange), 25% (yellow), 30% (red) and 35% (brown) v/v ethanol/toluene.

3.7. Complexation of analogous dyes with HAuCl₄

In an effort to provide further examples of this novel process and to develop a variety of new dye-functionalized GNPs, the scope of this methodology was explored with the structurally-related dye analogues **2-5**. Indeed, using the standard protocols for the complexation, we found that the dyes **2-4** gave rise to the corresponding GNP@**2-4**, respectively, while **5** failed under the identical conditions. As demonstrated experimentally with GNP@**1**, spectral measurements indicated the production of GNP@**2-4**, which exhibited obvious SPR bands at 515, 511 and 523 nm, respectively, in the absorption spectra (Fig. 5A-C) as well as strong fluorescence quenching of every excited chromophore in the fluorescence spectra (details in the Supplementary material, see Fig. S5A-C). On the contrary, in the case of the **5**-HAuCl₄ complex, we were reproducibly unable to detect significant level of SPR band in the absorption spectrum (Fig. 5D), nor to observe strong quenching of the excited anthracene chromophore in the fluorescence spectrum (Fig. S5D), although significant bathochromic shifts in the absorption maxima and decrease in the fluorescence emission, probably due to aggregation state of the chromophoric assemblies, were observed. As is apparent from the foregoing discussion, these observations can be understood on the basis of the lack of GNP

15

formation within molecular aggregates of the diprotonated **5**, indicating that the major factor responsible for the course of the chemical reaction should be the size of the hydrophilic pocket of the reverse micelles. In agreement with this proposal, it has been observed that **5** gave much smaller reverse micelles than those prepared from **2** when treated with sulfuric acid in toluene [19]. From these considerations, we conclude that the lack of the reactivity of **5** is possibly due to its unfavorable geometrical parameters for the formation of reactive sites required to promote the reductive processes.
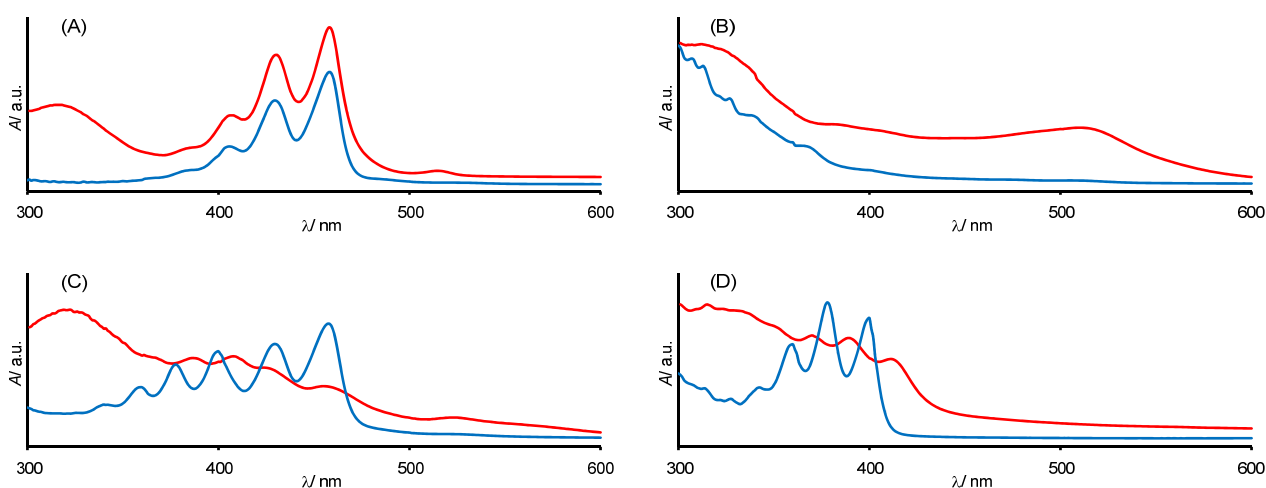
Fig. 5. Absorption spectra of dyes (blue) and their incubated samples (red) in toluene (dye represents **2** in (A), **3** in (B), **4** in (C) and **5** in (D), respectively).

3.8. AFM investigation of the new dye-functionalized GNP systems

For particle size estimation, dynamic light scattering (DLS) and transmission electron microscopy (TEM) measurements have been performed on the dye-functionalized GNPs. However, attempts to record appropriate size distributions failed primary due to undesirable formation of micrometer-scale aggregates of the dye-functionalized GNPs in sufficiently high concentrations to operate at distinct intensity levels. Therefore, we undertook atomic force microscopic (AFM) measurements of GNP@**2-4** as one of the most promising analytical methods available to survey their nanoscopic features (Fig. 6A-C). As has been observed with GNP@**1** [18], dispersed spherical objects were

detected on the highly oriented pyrolytic graphite (HOPG) substrate, which can be attributed to the individual dye-functionalized GNPs. Furthermore, cross-sectional views for these samples showed that the small spherical objects appeared to have average peak heights of about 7 nm (GNP@**2**), 2 nm (GNP@**3**) and 10 nm (GNP@**4**), respectively. From comprehensive evaluation of all detected spherical peaks collected by multiple scans, we found that nearly all the peaks gave the heights less than 20 nm (GNP@**2**), 10 nm (GNP@**3**), and 20 nm (GNP@**4**), respectively. These results suggest the dye-functionalized GNPs diffusing in the isotropic toluene medium adopt the stable globular structures with reasonably narrow diameter distributions centered on the nanoscopic dimension. On the other hand, AFM analysis of the **5**-HAuCl$_4$ complex showed structurally ill-defined or amorphous objects that differed significantly from the others (Fig. 6D). This result definitely indicates the failure of this material to form spherically shaped nanoparticles as well as some design criteria for the development of new types of dye-functionalized GNPs.
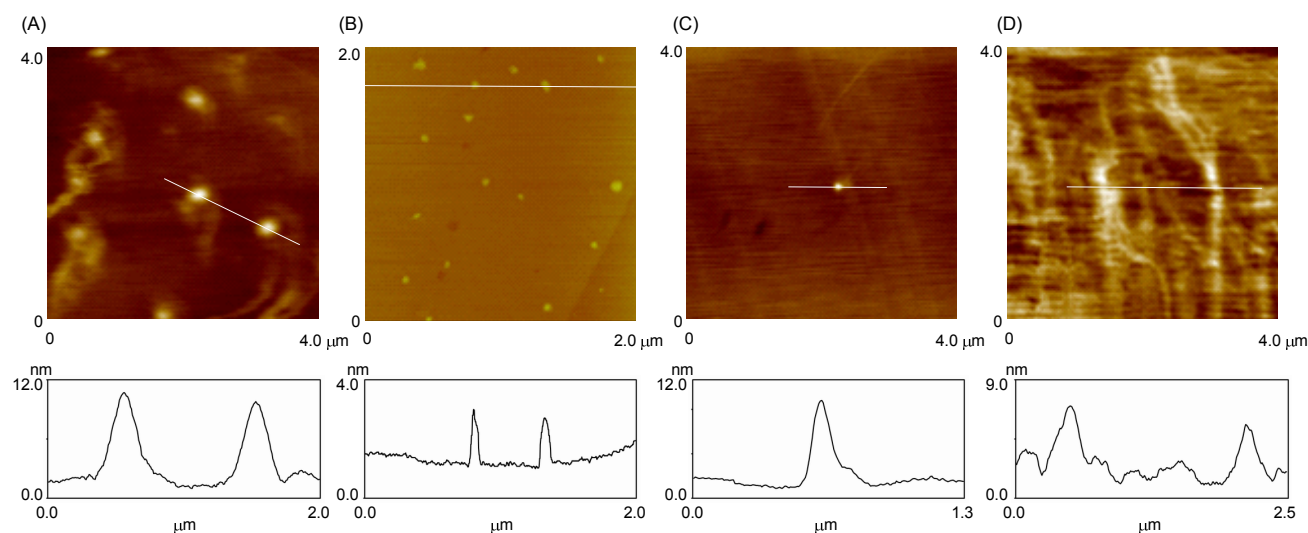
Fig. 6. AFM images and of drop-cast of (A) GNP@**2**, (B) GNP@**3**, (C) GNP@**4** and (D) **5**-HAuCl$_4$ complex (top) and their height profiles on cross-sections of the white solid lines in the corresponding AFM images (bottom).

3.9. Film-forming properties of the dye-functionalized GNPs

The resulting dye-functionalized GNPs exhibited good solubilities in a variety of organic solvents and showed excellent film-forming properties, offering optically homogeneous polystyrene thin films suitable for spectroscopic measurements. Fig. S6 (Supplementary material) depicts typical examples of absorption and fluorescence emission spectra of the GNP-doped polystyrene films. As can be seen in Fig. S6A, two types of pale yellow thin films prepared with GNP@**1** in toluene and in 35% v/v ethanol/toluene exhibited distinguishable shoulders assignable to the SPR bands at around 520 nm along with bathochromically shifted absorption spectra probably due to the chromophore aggregates. Meanwhile, another example of a thin film prepared from the toluene solution of GNP@**3**, which has a pink or pale reddish color, showed closely overlapping spectral feature relative to the solution spectrum. The above results imply that the size distributions of the GNPs observed in the toluene solution should be preserved in the polymer matrices with the aid of the reverse micellar shells of the dyes. Steady-state fluorescence measurements of the two thin films of GNP@**1** showed significantly different spectral behavior regarding a degree of fluorescence quenching of the excited perylene groups, as observed for the solution samples. In the fluorescence spectrum of the thin film prepared from the ethanol/toluene mixed solution (Fig. S6B), there appeared new emission bands in the longer wavelength region with distinct maxima at 498 and 533 nm as well as weak emission band of the monomeric perylene chromophores with a maximum at 465 nm, while complete quenching of the perylene emissions occurred in the other thin film system. From our experience [17], the new emission spectrum observed in the longer wavelength region can be attributed to excimer-like interacting perylene chromophores formed as a result of partial collapse of the swollen GNP@**1**. The results of the spectroscopic investigations confirm that the GNPs stabilized by the reverse micellar shells should maintain their inherent size and photophysical properties, even in the dried three-dimensional network of polystyrene.

4. Conclusions

In conclusion, we have investigated fundamental mechanistic aspects of the spontaneous formation of the dye-functionalized GNPs in the reverse micellar systems as well as further extension of this methodology to a variety of newly designed dyes. The accumulated results from the spectroscopic and microscopic investigations led to the following conclusions: (i) self-assembly of diprotonated dyes into the reverse micelles is an essential prerequisite for the spontaneous formation of GNPs, (ii) the GNPs generated in the reverse micelles are assumed to have approximately constant size distributions independent of the amount of $HAuCl_4$ as well as the water content added, (iii) the dye molecules remain essentially unchanged under the redox conditions and can be reproduced by the basic treatment, (iv) water molecules and/or polyols confined within the nanoscopic enclosure of the reverse micelles play a significant role during the course of the spontaneous reduction of aurate ions, (v) the dye-functionalized GNPs can provide the ability to tune their absorption and fluorescence emission characteristics simply by changing the medium polarity, (vi) the synthetic methodology to generate GNPs has potential applications for several dye analogues, (vii) the resulting dye-functionalized GNPs exhibit excellent film-forming properties to give optically homogeneous polystyrene thin films. These key findings demonstrate that the self-assembling process should serve as a potentially versatile access to a range of designed dye-functionalized GNPs without the need for any reducing agent, offering broad applicability of the resulting nanocomposites for device fabrication. Finally, we believe that continuing elaboration of the synthetic methods illustrated here will provide a potential convenience for the future development of new organic-inorganic hybrid nanomaterials [24, 25].

Appendix A. Supplementary material

Supplementary data associated with this article can be found, in the online version, at doi: xx/j.jcis.xx.

Schemes
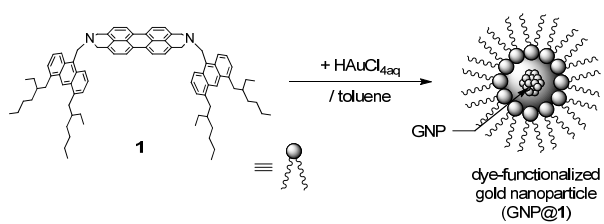
Scheme 1. Schematic representation of the production of the dye-functionalized GNPs from **1**.
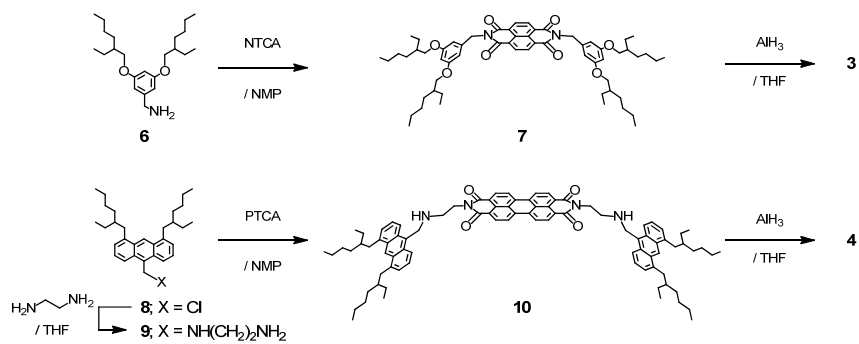
Scheme 2. Preparation of **3** and **4**.

Figures
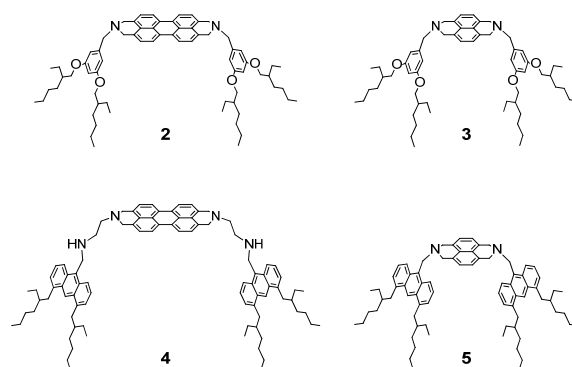
Fig. 1. Structures of dyes **2**-**5**.

Fig. 2. (A) Absorption (c = 10.0 µM) and (B) fluorescence (λ_{ex} = 368 nm, c 0.1 µM) spectra of **1** (blue) and dye-functionalized GNPs (red) in toluene. Red dotted line represents the enlarged fluorescence spectrum of the dye-functionalized GNPs in toluene.

Fig. 3. Absorption spectra of **1**-HAuCl$_4$ complexes in toluene at the c values of 0.1 (blue), 0.2 (light blue), 0.3 (green), 0.4 (light green), 0.5 (orange) and 1.0 mM (red) after incubation for 6 h.
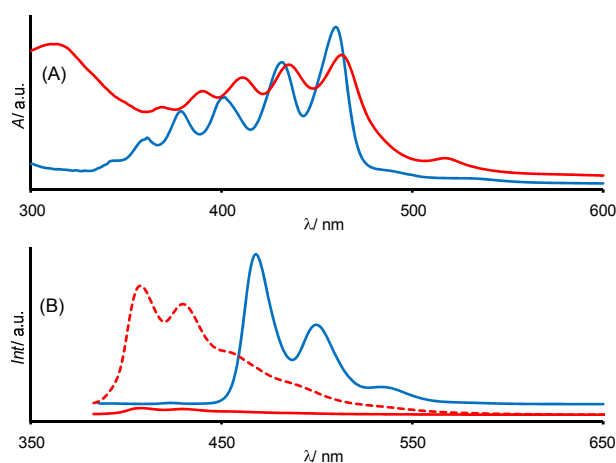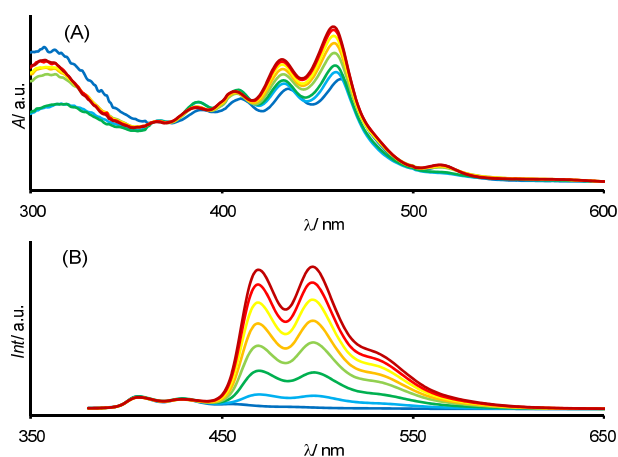
Fig. 4. (A) Absorption ($c = 10.0$ μM) and (B) fluorescence ($\lambda_{ex} = 368$ nm, $c = 0.1$ μM) spectra of dye-functionalized GNPs diluted with toluene (blue) and a mixture of 5% (light blue), 8% (green), 15% (light green), 20% (orange), 25% (yellow), 30% (red) and 35% (brown) v/v ethanol/toluene.
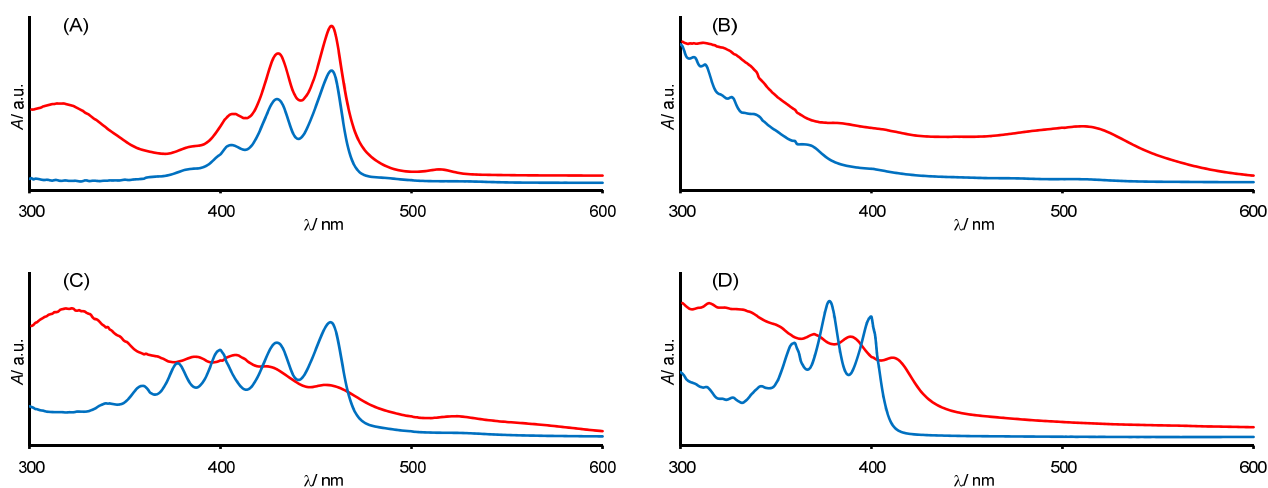
Fig. 5. Absorption spectra of dyes (blue) and their incubated samples (red) in toluene (dye represents **2** in (A), **3** in (B), **4** in (C) and **5** in (D), respectively).
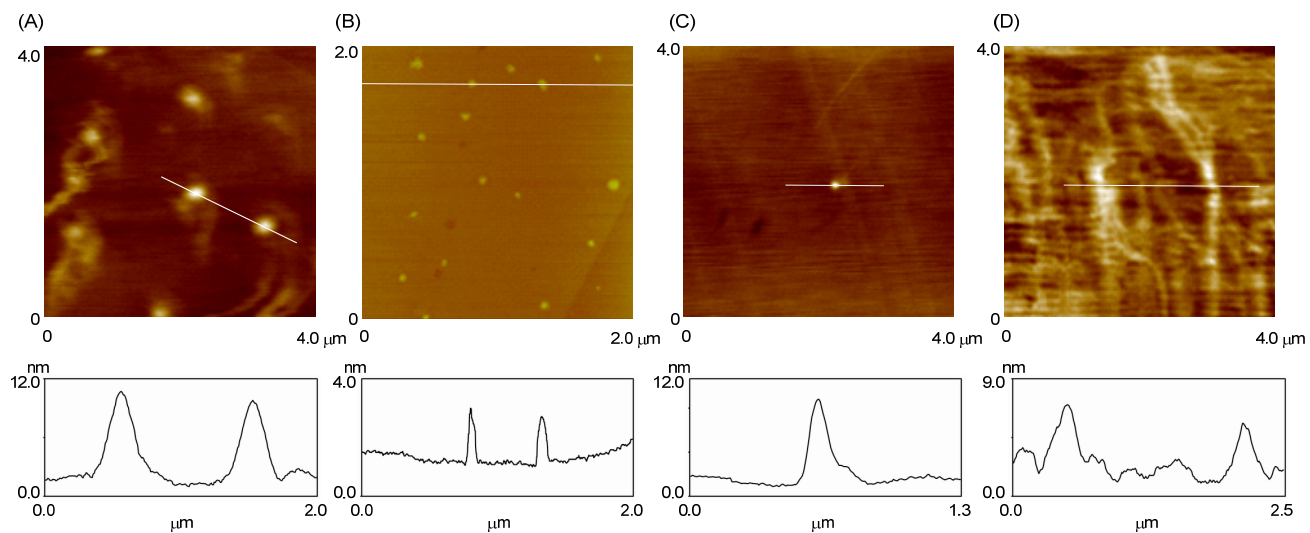
Fig. 6. AFM images and of drop-cast of (A) GNP@**2**, (B) GNP@**3**, (C) GNP@**4** and (D) **5**-HAuCl$_4$ complex (top) and their height profiles on cross-sections of the white solid lines in the corresponding AFM images (bottom).

References

[1] P. N. Prasad, Nanophotonics, John Wiley & Sons, Inc., Hoboken, NJ, 2004.

[2] K. M. L. Taylor-Pashow, J. D. Rocca, R. C. Huxford, W. Lin, Chem. Commun. 46 (2010) 5832.

[3] C. R. Kagan, D. B. Mitzi, C. D. Dimitrakopoulos, Science 286 (1999) 945.

[4] L. Sheeney-Haj-Ichia, B. Basnar, I. Willner, Angew. Chem. Int. Ed. 44 (2005) 78.

[5] L. Hu, Y. –L. Zhao, K. Ryu, C. Zhou, J. F. Stoddart, Adv. Mater. 20 (2008) 939.

[6] T. Cassagneau, J. H. Fendler, T. E. Mallouk, Langmuir 16 (2000) 241.

[7] A. Kira, T. Umeyama, Y. Matano, K. Yoshida, S. Isoda, M. Isosomppi, N. Tkachenko, H. Lemmetyinen, H. Imahori, Langmuir 22 (2006) 5497.

[8] Y. Chen, L. Chen, G. Qi, H. Wu, Y. Zhang, L. Xue, P. Zhu, P. Ma, X. Li, Langmuir 26 (2010) 12473.

[9] J. Méndez, R. Caillard, G. Otero, N. Nicoara, J. A. Marín-Gago, Adv. Mater. 18 (2006) 2048.

[10] I. Nabiev, A. Rakovich, A. Sukhanova, E. Lukashev, V. Zagidullin, V. Pachenko, Y. P. Rakovich, J. F. Donegan, A. B. Rubin, A. O. Govorov, Angew. Chem. Int. Ed. 49 (2010) 7217.

[11] A. Murray, W. L. Barnes, Adv. Mater. 19 (2007) 3771.

[12] K. Ueno, S. Juodkazis, T. Shibuya, Y. Yokota, V. Mizeikis, K. Sasaki, H. Misawa, J. Am. Chem. Soc. 130 (2008) 6928.

[13] R. A. Pala, J. White, E. Barnard, J. Liu, Adv. Mater. 21 (2007) 1.

[14] F. Gröhn, B. J. Bauer, Y. A. Akpalu, C. L. Jackson, E. J. Amis, Macromolecules 33 (2000) 6042.

[15] M. Zhu, N. Garg, M. E. Bier, R. Jin, J. Am. Chem. Soc. 130 (2008) 1138.

[16] C. Boyer, M. R. Whittaker, M. Luzon, T. P. Davis, Macromolecules 42 (2009) 6917.

[17] M. Takahashi, Y. Ichihashi, N. Nishizawa, S. Ohno, N. Fujita, M. Yamashita, T. Sengoku, H. Yoda, J. Photochem. Photobiol. A: Chem. 203 (2009) 56.

[18] M. Takahashi, S. Ohno, N. Fujita, T. Sengoku, H. Yoda, Chem. Lett. 39 (2010) 504.

[19] M. Takahashi, N. Nishizawa, S. Ohno, M. Kakita, N. Fujita, M. Yamashita, T. Sengoku, H. Yoda, Tetrahedron 65 (2009) 2669.

[20] T. Niwa Inada, K. Kikuchi, Y. Takahashi, H. Ikeda, T. Miyashi, J. Photochem. Photobiol. A: Chem. 137 (2000) 93.

[21] F. Bonet, C. Guéry, D. Guyomard, R. Herrera Urbina, K. Tekaia-Elhsissen and J. –M. Tarascon, Int. J. Inorg. Mater. 1 (1999), 47.

[22] L. Longenberger, G. Mills, J. Phys. Chem. 99 (1995) 475.

[23] S. Si, E. Dinda, T. K. Mandal, Chem. Eur. J. 13 (2007) 9850.

[24] M. –C. Daniel, D. Astruc, Chem. Rev. 104 (2004) 293.

[25] S. K. Ghosh, T. Pal, Chem. Rev. 107 (2007) 4797.